Available online at www.sciencedirect.com
ScienceDirect
Journal of Molecular Catalysis A: Chemical 261 (2007) 306–317
JOURNAL OF MOLECULAR CATALYSIS A: CHEMICAL
www.elsevier.com/locate/molcata

Active catalytic centers in silica-supported Cu(II) and Mn(II) biomimetic complexes: Correlation between catalytic and EPR data

Dimitris Zois [a], Chrysoula Vartzouma [a], Yiannis Deligiannakis [b], Nick Hadjiliadis [a], Luigi Casella [c], Enrico Monzani [c,*], Maria Louloudi [a,*]

[a] *Department of Chemistry, University of Ioannina, 45110 Ioannina, Greece*
[b] *University of Ioannina, Department of Environmental and Natural Resources Management, Laboratory of Physical Chemistry, Pyllinis 9, 30100 Agrinio, Greece*
[c] *Dipartimento di Chimica Generale, Università di Pavia, 27100 Pavia, Italy*

Received 4 May 2006; received in revised form 15 November 2006; accepted 16 November 2006
Available online 19 November 2006

Abstract

Two polydentate ligands represented as L_A and L_B have been synthesized and subsequently grafted on a silica surface via covalent bonds. The organic ligands L_A and L_B as well as the heterogenized ligands $L_A{\cdot}SiO_2$ and $L_B{\cdot}SiO_2$ reacted with manganese(II) and copper(II) ions leading to the formation of the corresponding metal complexes. Catalytic epoxidations of simple olefins with hydrogen peroxide were studied using the above manganese complexes in the presence of a cocatalyst. The major products of the oxidations were the epoxides and the studied manganese complexes showed significant catalytic activities. The copper(II) complexes have been evaluated for the catalytic oxidation of 3,5-di-*t*-butylcatechol (DTBC) by dioxygen. Based on a combination of structural information, obtained form EPR spectroscopy, and the catalytic activity we suggest that the catalysis of DTBC oxidation by copper complexes is critically determined by two factors (a) for dinuclear complexes, it is enhanced when the Cu···Cu distance approaches the OC···CO distance in the catechol molecule (2.7 Å), and (b) immobilization on silica support results in enhancement of the catalytic activity in cases where even monomeric complexes are located at relative distances approaching the critical OC···CO distance (2.7 Å). This provides a practical rule for design and synthesis of more efficient copper-catalysts for the catechol oxidation.

Keywords: Supported complexes; Copper and manganese complexes; Biomimetic catalysis; EPR and HYSCORE spectra; Alkene epoxidation; Catechol oxidation; DTBQ

1. Introduction

The heterogenization of catalysts, in our environmentally conscious days, provides important 'green benefits' when solvent losses and catalyst losses on separation can lead to unacceptable levels of waste [1]. The use of inorganic support materials with chemically bound active centres as heterogenized catalysts endows the homogeneous systems with attractive features such as easy product separation, and catalyst stability and recovery [2,3]. A range of possible synthetic procedures exists for attaching organic functionalities to the surface of a support [4]. The fixation of active biomimetic ligands via covalent attachment to a silica surface for catalytic processes presents a remarkable aspect of this concept. Functionalized alkoxysilanes such as 3-aminopropyltriethoxysilane [5], 3-sulfanylpropyltrimethoxysilane [6], mono-ethoxydimethylsilyl-butanal [7], cyanoethyltriethoxylsilane [8], 3-(triethoxy-silyl) propyl isocyanate [9], (3-glycidyloxypropyl)trimethoxysilane [10] or iodopropyltrimethoxysilane [11] have been used as connecting links. It has been suggested that functionalization takes place mainly at the hydrophobic regions of the silica surface, involving surface siloxane bridges, and occurs through a nucleophilic displacement at the silicon atom by the alkylsiloxane group of the silylating agent [12]. The functional ligands should be easy to prepare by simple, available starting materials and amenable to facile chemical modifications [13]. Their incorporation on the inorganic support has to be easily accomplished with minimum structural changes. Polynitrogenated compounds fulfill such requirements and they are able to bind metal ions

* Corresponding authors. Tel.: +30 26510 98418; fax: +30 26510 44831.
E-mail addresses: emonzani@unipv.it (E. Monzani), mlouloud@uoi.gr (M. Louloudi).

1381-1169/$ – see front matter © 2006 Elsevier B.V. All rights reserved.
doi:10.1016/j.molcata.2006.11.023

selectively among their various oxidation states [14]. Thus, a number of nitrogen ligands immobilized on silica support have been prepared and the corresponding transition-metal-incorporated materials promoted oxidation reactions [15].

The epoxidation of olefins is a particularly challenging problem in organic chemistry, due to the utility of epoxides as synthetic intermediates. Manganese complexes with various bioinspired ligands can potentially act as catalysts for oxidation of alkenes using H_2O_2 as oxidant [16–21]. Nevertheless, the catalytic activity of these complexes is limited by their tendency to decompose H_2O_2. However, it has been shown that peroxide disproportionation is suppressed in acetone favouring alkene epoxidation [22–24]. In the presence of H_2O_2, the use of a supported manganese catalyst instead of a homogeneous one, leads to additional problems related to the possible dismutation of H_2O_2 by the inorganic support. These considerations would explain why only a few systems based on supported manganese catalysts and H_2O_2 have been reported for alkene oxidation [10,25].

As far as catechol oxidation by copper complexes is concerned, several mononuclear and dinuclear copper complexes have been studied, investigating their reactivity towards dioxygen [26–34]. These copper compounds have served as models for the active sites of copper proteins and the observed biomimetic activity has been correlated to their structural features [26–34].

Herein we describe the synthesis and immobilization of two new polydentate ligands on a silica surface. Their grafting is achieved via covalent bonding to the inorganic support. It is shown that the supported manganese complexes catalyze efficiently the epoxidation of several alkenes by hydrogen peroxide in the presence of ammonium acetate as cocatalyst, even under mild conditions. The catalytic activities of the silica supported Cu(II) complexes were evaluated for the oxidation of 3,5-di-*t*-butylcatechol by air dioxygen. Catalytic data and structural information obtained by EPR spectra are correlated and discussed.

2. Experimental

All substrates were purchased in their highest commercial purity, stored at 5 °C and purified by passage through a column of basic alumina prior to use. Hydrogen peroxide was 30% solution in water.

Infrared spectra were recorded on a Spectrum GX Perkin–Elmer FT-IR System, UV–vis spectra were recorded using a UV–vis/NIR JASCO Spectrophotometer. ESI-MS spectra were obtained from a Finnigan MAT system equipped with an ion trap detector and solution NMR spectra were recorded with a Bruker AMX-400 MHz spectrometer with external TMS as reference. Room temperature magnetic susceptibilities were measured by Evans's method using a Johnson Matthey balance standardized with $HgCo(NCS)_4$; corrections for the diamagnetism of the complexes were estimated from Pascal's constants. Diffuse reflectance UV–vis spectra were recorded at room temperature on a Shimadzu UV-2401PC with a $BaSO_4$ coated integration sphere. Thermogravimetric analyses were carried out using Shimadzu DTG-60 analyser. High performance liquid chromatography (HPLC) analysis was performed using a Dionex liquid chromatograph equipped with a C18 column, the eluent being a mixture of methanol and water (30/70, v/v) at a flow rate of 0.6 ml min^{-1}, detection at 280 and 418 nm. GC analysis was performed using an 8000 Fisons chromatograph with a flame ionization detector and a Shimadzu GC-17A gas chromatograph coupled with a GCMS-QP5000 mass spectrometer.

2.1. EPR and ESEEM spectra

Continuous-wave (c.w.) EPR spectra were recorded at liquid helium temperatures with a Bruker ER 200D X-band spectrometer equipped with an Oxford Instruments cryostat. The microwave frequency and the magnetic field were measured with a microwave frequency counter HP 5350B and a Bruker ER035M NMR-gaussmeter, respectively. Orientation-selective pulsed EPR experiments were performed with a Bruker ESP380 spectrometer with a dielectric resonator. In the three-pulse ($\pi/2$-τ-$\pi/2$-T-$\pi/2$) electron spin echo envelope modulation (ESEEM) spectra [35] the amplitude of the stimulated echo as a function of $\tau + T$ was measured at a frequency near 9.6 GHz at various magnetic field settings across the field-swept Echo-detected EPR spectrum. Data manipulations were performed as described earlier [36].

Two-dimensional (2D) hyperfine sublevel correlation spectroscopy (HYCORE) spectra [37] recorded for the Cu^{2+} complexes studied here contained cross-peaks from nuclear transitions corresponding to either ^{14}N, or ^{1}H, some of them having considerable hyperfine anisotropy. For each complex, several HYSCORE spectra were recorded at various τ-values, in order to compensate for the blind-spots due to τ-suppression effect [35]. Thus, the frequency domain HYSCORE spectra recorded at $\tau = 88$, 120 and 136 ns (all the other experimental parameters being kept similar) were added together in order to minimize blind-spots. The HYSCORE spectra were recorded at 3351G corresponding to the $g_\perp$ orientations.

We have carefully verified that exhaustive washing of the $Cu(L)\cdot SiO_2$ materials eliminates interference from background signals, i.e. for Cu(II) adsorbed at he SiO_2 surface in the absence of the ligands L_A, L_B.

2.2. Synthesis of the ligand 2-(3H-imidazol-4-yl)-N-[2-(3H-imidazol-4-yl)-ethyl]-acetamide (*L*$_A$) and its Mn(II) and Cu(II) complexes

2.2.1. 2-(3H-Imidazol-4-yl)-N-[2-(3H-imidazol-4-yl)-ethyl]-acetamide (L_A)

1.5 mmol of the sodium salt of 4-imidazoleacetic acid and 3.0 mmol of $SOCl_2$ were added in a pyridine solution (25 ml). The resulting mixture was refluxed under N_2 for 2 h. Then 1.5 mmol of histamine dihydrochloride were added into the reaction mixture, which was stirred at 75–80 °C under N_2 for 12 h. After evaporating the solvents, the ligand was isolated as a solid. The final product was obtained by recrystallization from methanol and ethanol, respectively. Anal. Calcd. for $C_{10}H_{13}N_5O\cdot 2HCl$ (%): C, 43.10; N, 14.0; H, 5.0. Found (%): C, 42.7; N, 14.3; H, 5.0. IR (KBr,

cm^{-1}, selected peaks) 3413: ((NH); 3139, 3050, 3034, 2901: ν(CH); 1683: ν(C=O)(amide I); 1549: ν(C–N) (amide II); 1483, 1443, 1410: CH and ring stretching modes (imidazole); 1261: δ(NH) (amide III); 664: (N–C=O) deformation (amide IV). ^{1}H NMR (CD_3OD, () 8.7 (d): (Im–**H**); 7.4 (d): (Im–**H**); 3.9 (s): C=O–C**H$_2$**–Im; 3.4 (t): C=O–NH–C**H$_2$**–CH_2–Im; 3.2 (t): C=O–NH–CH_2–C**H$_2$**–Im. ^{13}C NMR (CD_3OD, δ) 175: **C**O; 136 (d): **C**=N (Im); 129 (d), 119 (d): **C**=**C** (Im) ; 40: C=O–**C**H_2–Im; 32: C=O–NH–**C**H_2–CH_2–Im; 24: C=O–NH–CH_2–**C**H_2–Im. ESI-MS (*m/z)* 220 ($[MH]^+$); 256 ($[MH + HCl]^+$). UV (MeOH, λ_{max} (nm), ε (M^{-1} cm^{-1})) 238 (14 000); 266 (35 000); 276 (42 000).

2.2.2. *[$Mn_2(CH_3COO)_4(L_A)$], (1)*

To a stirred solution of methanol (15 ml) containing the ligand L_A (1.5 mmol) and triethylamine (3.0 mmol), a solution of $Mn(CH_3COO)_2{\cdot}4H_2O$ (3.0 mmol) in methanol (10 ml) was added. The resulting mixture was stirred for 2 h at room temperature and a solid product was separated by the addition of small amounts of diethyl ether. The complex thus obtained, $[Mn_2(CH_3COO)_4(L_A)]$, was washed with small amounts of cold EtOH and dried under reduced pressure at 40 °C. Anal. Calcd. For $Mn_2C_{18}H_{25}N_5O_9$ (%): C, 38.25; N, 12.39; H, 4.45; Mn, 19.45. Found: C, 38.08; N, 11.86; H, 4.12; Mn, 19.04. IR (KBr, cm^{-1}, selected peaks): 3395: ν(NH); 1578: $\nu_{sym}(COO^-)$; 1409: $\nu_{as}(COO^-)$; 649: (N–C=O) deformation (amide IV). UV (MeOH, λ_{max} (nm), ε (M^{-1} cm^{-1})) 249 (10 500); 276 (21 000); 285 (27 000).

2.2.3. *[$Cu_2(ClO_4)_4(L_A)$], (2)*

The reaction of L_A with $Cu(ClO_4)_2.{\cdot}6H_2O$ by the same procedure as above leads to the formation of the $[Cu_2(ClO_4)_4(L_A)]$ complex. Anal. Calcd. For $Cu_2C_{10}H_{13}N_5O_{17}Cl_4$ (%): C, 16.14; N, 9.41; H, 1.76; Cu, 17.09. Found: C, 15.96; N, 9.24; H, 1.58; Cu, 16.85. IR (KBr, cm^{-1}, selected peaks): 3378: ν(NH); 3123, 3028, 2899: ν(CH); 1656: ν(C=O) (amide I); 1534: ν(C–N) (amide II); 1476, 1431, 1401: CH and ring stretching modes (imidazole); 1244: δ(NH) (amide III); 1104: $\nu(ClO_4^-)$. ESI-MS (*m/z*) 644.5 ($[Cu_2L_A(ClO_4)_3]^+$). UV–vis (MeOH, λ_{max} (nm), ε (M^{-1} cm^{-1})) 251 (9 500); 279 (16 000); 292 (22 000); 689 (23).

2.3. *Immobilization of (L_A) on a silica support and the preparation of the supported $Mn_2(L_A){\cdot}SiO_2$ and $Cu_2(L_A){\cdot}SiO_2$ complexes*

2.3.1. *$L_A{\cdot}SiO_2$*

To a stirred solution of 80 ml toluene containing 1.0 mmol of L_A, 1.0 mmol of (3-glycidyloxypropyl)-trimethoxysilane was added. The resulting mixture was allowed to react at 80 °C for 24 h. To this solution 1.5 g of SiO_2 and 5 ml of EtOH were added, and the slurred solution was maintained at 80 °C for 24 h. The functionalized silica, $L_A{\cdot}SiO_2$, was isolated by filtration and washed with MeOH and EtOH. It was further purified with EtOH using the soxhlet extraction method and dried under reduced pressure at 50 °C for 12 h. The loading achieved is ca. 0.5 mmol g^{-1}, as determined by thermogravimetric analysis. DRIFTS-IR (cm^{-1}, selected peaks): 2982: ν(CH); 1684: ν(C=O)(amide I); 1485, 1448, 1396: CH and ring stretching modes (imidazole). DRS (λ_{max} (nm)): 268; 289.

2.3.2. *$Mn_2(L_A){\cdot}SiO_2$, (3)*

To a suspension of $L_A.SiO_2$ (1.7 g) in MeOH, $Mn(CH_3COO)_2{\cdot}4H_2O$ (2 mmol) was added. The mixture was stirred for 24 h at room temperature and the resulting material, $Mn_2(L_A){\cdot}SiO_2$, was filtered, washed thoroughly with EtOH and Et_2O and dried at 50 °C for 12 h. The amount of Mn^{II} was determined by back-titration of the remaining amount of Mn^{II} into the filtrate and the collected washings. The ratio between the immobilized organic component and the coordinated metal ion was found to be 1:2. DRIFTS-IR (cm^{-1}, selected peaks): 1581: $\nu_{sym}(COO^-)$; 1416: $\nu_{as}(COO^-)$. DRS (λ_{max} (nm)): 279; 298.

2.3.3. *$Cu_2(L_A).SiO_2$, (4)*

Following the same synthetic procedure as for $Mn_2(L_A){\cdot}SiO_2$ and using $Cu(ClO_4)_2{\cdot}6H_2O$ as metal salt, the supported metal complex, $Cu_2(L_A){\cdot}SiO_2$, has been prepared. DRIFTS-IR (cm^{-1}, selected peaks): 2985: ν(CH); 1483, 1441, 1387: CH and ring stretching modes (imidazole). DRS (λ_{max} (nm)): 270; 308; 692.

2.4. *Synthesis of the ligand bis(benzimidazol-2-ylmethyl) amine monohydrate (L_B) and its Mn(II) and Cu(II) complexes*

2.4.1. *Bis(benzimidazol-2-ylmethyl)amine monohydrate (L_B)*

Iminodiacetic acid (0.01 mol) and 1,2-diaminobenzene (0.2 mol) were intimately mixed and heated to 180–200 °C (oil-bath) in an open flask. When no further steam was evolved the melt was allowed to cool. The dark glassy solid was taken up in hot hydrochloric acid (0.4 mol/l, 20 ml) and filtered. After cooling, the ligand precipitated as a pale blue, feathery solid. This was taken up in warm water (20 ml), KOH (0.5 mol) added, and the solution brought to reflux. Methanol was added until the precipitate redissolved. After refluxing with decolourizing charcoal (15 min) the solution was filtered and gave the crude free amine upon cooling. Two recrystallizations from methanol–water gave the ligand as white needles. Anal. Calcd. for $C_{16}H_{15}N_5{\cdot}H_2O$ (%): C, 65.10; N, 23.70; H, 5.80. Found (%): C, 65.20; N, 23.70; H, 5.80. The amount of water present in the compound was also confirmed from the TG patterns. IR (KBr, cm^{-1}, selected peaks) 3408: ν(OH) (water molecule); 3238: ν(NH); 3053, 2924: ν(CH); 1645, 1622, 1540, 1459, 1439: ring and CH stretching vibrations (benzimidazole); 1279: ν(C–N) (secondary amine); 738: CH deformation modes. ^{1}H NMR (CD_3OD, δ) 7.5 (m): (Bim–**H**); 7.2 (m): (Bim–**H**); 4.1 (s): Bim–C**H$_2$**–NH–C**H$_2$**-Bim. ^{13}C NMR (CD_3OD, δ) 148: N–**C**=N (Bim); 137: =**C**= (Bim); 121, 116: –**C**H– (Bim); 50: Bim–**C**H_2–NH–**C**H_2–Bim. ESI-MS (*m/z)* 278 ($[MH]^+$); 300 ($[M + Na]^+$). UV (MeOH, λ_{max} (nm), ε (M^{-1} cm^{-1})) 239 (27 500); 271 (31 000); 279 (36 500).

2.4.2. $[Mn(CH_3COO)_2(L_B)]\cdot H_2O$, (5)

The ligand L_B (1 mmol) was dissolved in a 1:1 mixture of methanol and dichloromethane (20 ml) under stirring. Then, a solution of $Mn(CH_3COO)_2\cdot 4H_2O$ (1.0 mmol) in methanol (5 ml) was added. Within 20 min, a light brown precipitate formed. The mixture was concentrated under vacuum to about half volume, and the product was collected by filtration. The metal complex, $[Mn(CH_3COO)_2(L_B)]\cdot H_2O$ was obtained by recrystallization from ethanol and dried under reduced pressure at 40 °C. Anal. Calcd. For $MnC_{20}H_{21}N_5O_4\cdot H_2O$ (%): C, 51.29; N, 14.95; H, 4.95; Mn, 11.74. Found: C, 51.68; N, 15.14; H, 4.59; Mn, 11.43. The amount of water present in the complex was also confirmed from the TG patterns. IR (KBr, cm^{-1}, selected peaks): 3422: ν(OH) (water molecule); 3221: ν(NH); 3059, 2925: ν(CH); 1559: $\nu_{sym}(COO^-)$; 1455: $\nu_{as}(COO^-)$; 1274: ν(C–N) (secondary amine); 745: CH deformation modes. UV (MeOH, λ_{max} (nm), ε ($M^{-1}\,cm^{-1}$)) 248 (19 500); 276 (23 000); 287 (28 500).

2.4.3. $[Cu(ClO_4)_2(L_B)]\cdot H_2O$, (6)

This complex was prepared by the same method as for $[Mn(CH_3COO)_2(L_B)]\cdot H_2O$, but using $Cu(ClO_4)_2\cdot 6H_2O$ as metal salt, giving a blue solid. Anal. Calcd. For $CuC_{16}H_{15}N_5O_8Cl_2\cdot H_2O$ (%): C, 34.44; N, 12.56; H, 3.05; Cu, 11.40. Found: C, 34.18; N, 12.34; H, 3.10; Cu, 11.08. IR (KBr, cm^{-1}, selected peaks): 3409: ν(OH) (water molecule); 3226: ν(NH); 3059, 2919: ν(CH); 1621, 1594, 1532, 1452, 1427: ring and CH stretching vibrations (benzimidazole); 1262: ν(C–N) (secondary amine); 1113: $\nu(ClO_4^-)$; 738: CH deformation modes. ESI-MS (*m/z*) 339 ($[CuL_B\text{-}H]^+$, 70%), 439 ($[CuL_B(ClO_4)]^+$, 100%), 879 ($[Cu_2(L_B)(L_B\text{-}H)(ClO_4)_2]^+$, 20%), 979 ($[Cu_2(L_B)_2(ClO_4)_3]^+$, 30%). UV–vis (MeOH, λ_{max} (nm), ε ($M^{-1}\,cm^{-1}$)) 247 (14 500); 278 (21 000); 289 (21 500); 684 (180).

2.5. Immobilization of (L_B) on a silica support and the preparation of the supported $Mn_2(L_B)\cdot SiO_2$ and $Cu_2(L_B)\cdot SiO_2$ complexes

2.5.1. $L_B\cdot SiO_2$

For the functionalization of silica with L_B, the same procedure has been followed as in the case of L_A, by reacting 1.0 mmol of L_B with 1.0 mmol of (3-glycidyloxypropyl)-trimethoxysilane in 80 ml toluene. The resulting solution was allowed to react at 80 °C for 24 h. After the addition of 1.5 g of SiO_2 and 5 ml of EtOH to the reaction mixture, the resulting slurred solution was maintained at 80 °C for 24 h. The functionalized silica, $L_B\cdot SiO_2$, was isolated by filtration and washed with MeOH and EtOH. It was further purified with EtOH using the soxhlet extraction method and dried under reduced pressure at 50 °C for 12 h. The loading achieved is ca. 0.5 mmol g^{-1}, as determined by thermogravimetric analysis. DRIFTS-IR (cm^{-1}, selected peaks): 3055, 2945: ν(CH); 1657, 1641, 1533, 1510, 1463: ring and CH stretching vibrations (benzimidazole); 1284: ν(C–N) (secondary amine). DRS (λ_{max} (nm)): 232, 274; 286.

2.5.2. $Mn(L_B)\cdot SiO_2$, (7)

To a suspension of $L_B\cdot SiO_2$ (0.9 g) in MeOH, $Mn(CH_3COO)_2\cdot 4H_2O$ (0.5 mmol) was added. The mixture was stirred for 24 h at room temperature and the resulting supported complex, $Mn(L_B)\cdot SiO_2$, was filtered, washed thoroughly with EtOH and Et_2O and dried at 50 °C for 12 h. The amount of Mn^{II} was determined by back-titration of the remaining amount of Mn^{II} into the filtrate and the collected washings. The ratio between the immobilized organic component and the coordinated metal ion was found to be 1:1. DRIFTS-IR (cm^{-1}, selected peaks): 1572: $\nu_{sym}(COO^-)$; 1431: $\nu_{as}(COO^-)$; 1276: ν(C–N) (secondary amine). DRS (λ_{max} (nm)): 250; 278; 292.

2.5.3. $Cu(L_B)\cdot SiO_2$, (8)

This supported copper complex was prepared by the same method as for $Mn(L_B)\cdot SiO_2$ but using $Cu(ClO_4)_2\cdot 6H_2O$ as metal source. DRIFTS-IR (cm^{-1}, selected peaks): 3055, 2945: ν(CH); 1636, 1622, 1613, 1496, 1481, 1451: ring and CH stretching vibrations (benzimidazole); 1280: ν(C–N) (secondary amine). DRS (λ_{max} (nm)): 251, 279; 294; 687.

2.6. Analysis of the HYSCORE Spectra

In general, the frequency-domain HYSCORE spectra consist of correlation cross-peaks whose coordinates are nuclear frequencies ($\pm\nu_\alpha$, $\pm\nu_\beta$) from opposite electron spin manifolds [37]. The shape of the observed cross-peaks in copper complexes has been reviewed in detail [38].

The EPR spectra for the Cu^{2+} complexes studied here are characterized by axial **g**-tensors. In such case analytical expressions for the lineshapes of the $I = 1/2$, HYSCORE spectra have been derived previously [36] based on the method of Pöppl and Kevan [39]. We assume that the anisotropic electron–nuclear interaction can be described by the point-dipole approximation. In the ^{1}H-HYSCORE spectra for increasing hyperfine anisotropy there is a progressive spread of the cross-peaks which become arc-shaped [35–39] and a progressive increase of the maximum shift from the $(-\nu_I, \nu_I)$ antidiagonal. The maximum $\Delta\nu_{max}$ shift allows the estimation of the anisotropic hyperfine coupling (A_{ani}) [36,39].

$$A_{ani} \equiv g_\perp T = \frac{2}{3}\sqrt{\frac{8\Delta\nu_{max}\nu_I}{\sqrt{2}}} \quad (1a)$$

Having an estimate of A_{ani}, the isotropic hyperfine coupling A_{iso} can be estimated from the frequencies of the outer edges of the ridges, according to the relation [36,39]

$$A_{iso} = (\nu_\alpha - \nu_\beta) - 2A_{ani} \quad (1b)$$

The ^{14}N($I = 1$) HYSCORE cross peaks are analyzed assuming that they originate from the three ^{14}N nuclear transitions from each of the $m_s = \pm 1/2$ electron spin manifold [35,38]

2.7. Estimation of the Cu···Cu distance for SiO_2 immobilized complexes

In dimeric Cu^{2+} complexes the EPR spectral features depend on the spin–spin interaction [40]. If an efficient orbital overlap pathway is available, ligand-mediated superexchange interaction occurs [41,42]. Dipolar interactions result in "semi-forbidden," $\Delta M_S = 2$ transitions which in X-band EPR spectra are detected at "half-field" in the region 1500–1700 G. Eaton et al. [43] have demonstrated that in infinite diluted samples where intermolecular spin–spin interaction, from neighbouring complexes, is negligible the intensity of the half-field transition can be used for relatively accurate estimate of the distance between the coupled spins:

$$R_{\text{Angtroms}} = \sqrt[6]{\frac{A}{I}\left(\frac{9.1}{\nu}\right)^2} \tag{2a}$$

where

$$I = \frac{\text{Integrated Intensity of the } \Delta M_S = 2 \text{EPR signal}}{\text{Integrated Intensity of the } \Delta M_S = 1 \text{EPR signal}} \tag{2b}$$

the factor A is a fixed empirical constant which for Cu···Cu complexes is [43,44]

$$A = 20 \pm 1$$

This method has proven to give accurate results in Cu···Cu complexes (Fig. 1) for distances in the range of 4–6 Å [45].

The applicability of this method depends critically on the elimination of interferences from non-specific intermolecular spin–spin interactions from neighbouring complexes. In frozen solution this requires a series of EPR spectra to be recorded under non-saturating conditions for progressively more diluted spectra [43]. Based on these measurements, the spin–spin distance can be estimated by extrapolation to infinite dilution [43,45].

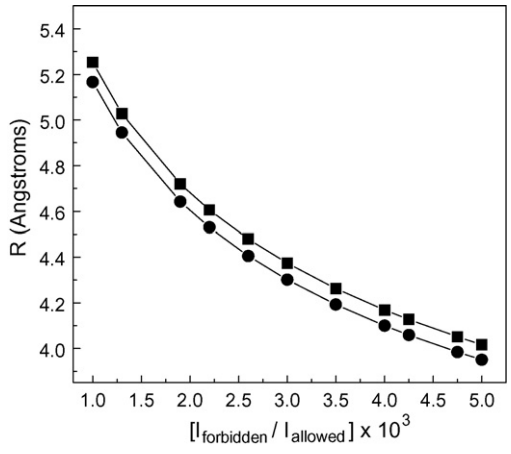

Fig. 1. Interspin distance R for a coupled $S_1 = 1/2$, $S_2 = 1/2$ spin pair as a function of the ratio of the integrated EPR signal intensity of the forbidden vs. the allowed transitions according to Eq. (2a), for two values of the parameter A: (■) $A = 21$, or (●) $A = 19$.

In the case of complexes immobilized onto SiO_2-particles the spin pairs, if present, will be fixed spatially. We assume that the immobilized complexes are homogeneously dispersed onto the SiO_2-particle at average distances determined by the loading of the silica particles. Lowering the loading will result in well-spaced complexes and this will eliminate non-specific intermolecular spin–spin interaction. Interparticle interactions are expected to play minor role. Therefore the SiO_2-grafted dimeric complexes at low loading are suitable for use of the formula (1a and 1b) for the calculation of the interspin distance by EPR spectroscopy. Such experiments would be of importance for further calibration of the validity of this approach in systems where the half-field transition is EPR detectable. Here we have applied this method for the $Cu_2(\mathbf{L_A})\cdot SiO_2$ and $Cu(\mathbf{L_B})\cdot SiO_2$ complexes.

2.8. Catalytic reactions

2.8.1. Alkene epoxidations

Hydrogen peroxide was slowly added to solution of alkene and cocatalyst in a acetone/MeOH (500/350 μl) solvent mixture at room temperature. As an internal standard, acetophenone or bromobenzene were used. Catalytic reactions were started by adding 1 μmol of corresponding manganese catalyst. The ratios of [catalyst:oxidant: cocatalyst:substrate] were equal to [1:2000:1000:1000].

The progress of the reaction was monitored by GC–MS, by removing small samples of the reaction mixture. Reactions were usually complete within 24 h. To establish the identity of the products unequivocally, the retention times and spectral data were compared to those of commercially available compounds.

2.8.2. DTBC oxidation

In a typical experiment, catalyst complex (0.3 ml of a 10^{-3} M methanol solution or the corresponding amount of the supported catalyst), and 300 μl of triethylamine (10^{-1} M methanol solution) were mixed with a 2.0 ml solution (10^{-1} M methanol solution) of 3,5-di-*tert*-butylcatechol. Aliquots were removed at appropriate time intervals for GC analysis or/and diluted 10 times with methanol for HPLC analysis. Blank experiments showed that without catalyst the transformation of DTBC to DTBQ does not take place.

Generally the heterogenized catalysts recovered by filtration from the catalytic reactions exhibited (a) identical IR spectra with the 'unused' catalysts and (b) almost the same loading determined by thermogravimetric analysis indicating that there is no leaching of the supported catalysts during the catalytic reactions. However, to furthermore ensure that no leaching of the active supported component occurs, the 'filtration method' is carried out according to Valkenberg and Hölderich [46]. Accordingly, in typical catalytic experiments, after 1 h, the solid catalysts were filtered. Into the filtrate, the progress of the oxidation reaction was monitoring by GC. No evolution of the studied reactions has been observed in the filtrate. Overall these data ensure that no leaching of the supported catalysts occurs.

3. Results and discussion

3.1. Synthesis and characterization of the ligands and their metal complexes

The acetamide derivative **L_A** containing two imidazole residues was prepared by activation of 4-imidazoleacetic acid with $SOCl_2$ and subsequent reaction with histamine (Scheme 1). The only isolated product exhibited an ESI-mass spectrum with a molecular peak $[MH]^+$ at *m/z* 220 and IR bands at 1683, 1549, 1261 and 664 cm^{-1}, attributable to the amide I, II, III and IV modes, respectively. ^1H and ^{13}C NMR data clearly suggested the formation of the ligand indicating the presence of two non-identical imidazole rings. In the near-UV region, the electronic spectrum of **L_A** comprised both acetamide and imidazole absorptions at 238, 266 and 276 nm.

The distribution of heteroatoms of the ligand **L_A** enables to obtain two metal coordination sites. The reaction of **L_A** with manganese(II) acetate and copper(II) perchlorate led to the formation of bimetallic $[Mn_2(CH_3COO)_4(L_A)]$ and $[Cu_2(ClO_4)_4(L_A)]$ complexes. In the ESI-MS spectrum, the $[Cu_2(ClO_4)_4(L_A)]$ complex showed a molecular peak $[Cu_2L_A(ClO_4)_3]^+$ at *m/z* 644.5. The MID- and FAR-IR data indicate metal coordination to the amide and imidazole nitrogens.

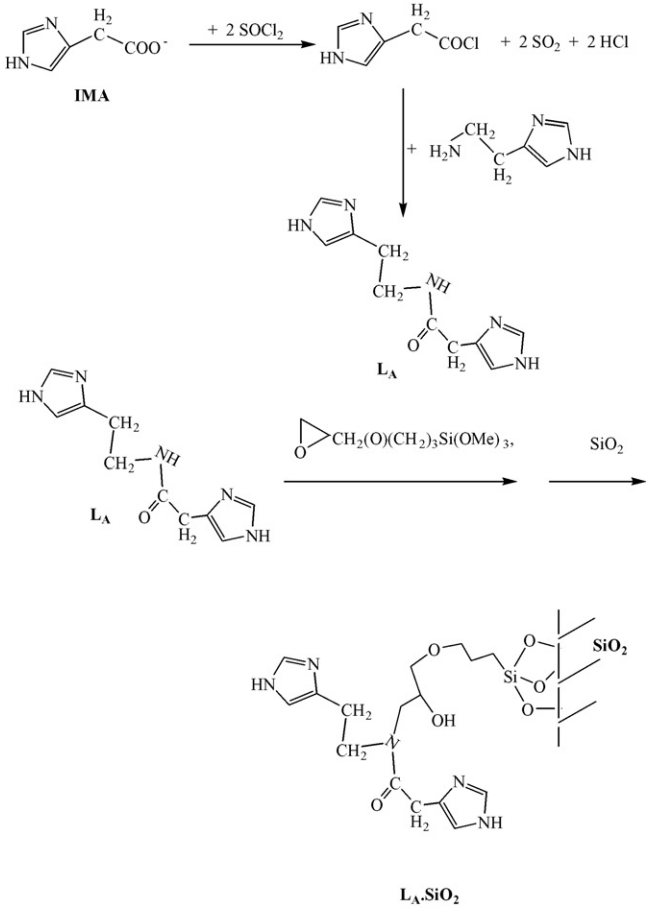

Scheme 1. Synthesis and immobilization of the ligand L_A.

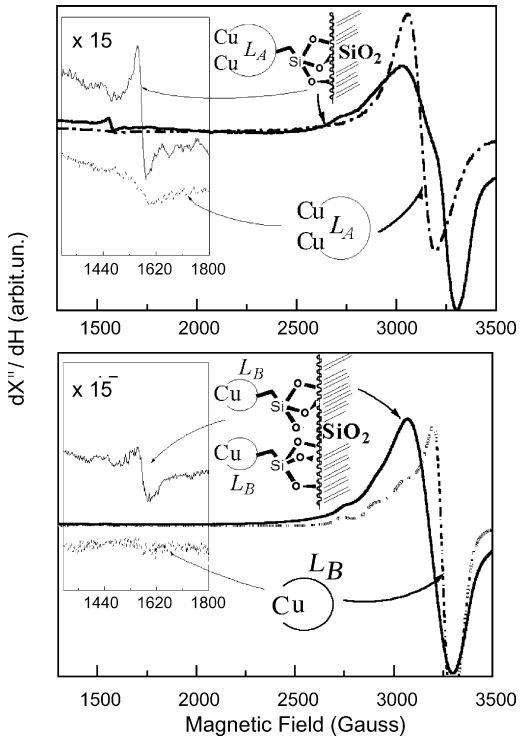

Fig. 2. Continuous wave EPR spectra for CuL_A (top) and CuL_B (bottom). (dashed lines) EPR spectra in frozen methanol. (solid lines) Powder EPR spectra for the immobilized complexes on SiO_2. The inset in each panel is an expanded scale, i.e., 15-fold, of the $\Delta M_S = 2$ region. Common EPR parameters $T = 4.5$ K, modulation amplitude 10 G, microwave power 32 mW.

The EPR spectrum of the manganese complex recorded at 4 K is characterized by a broad signal centered at $g \sim 2$, accompanied by forbidden ($\Delta M_S = 2$) transitions at $g = 4$ indicating antiferromagnetically coupled $Mn^{II}Mn^{II}$ dimers [47]. This is further supported by μ_{eff} value of this complex, which amounts to 5.27 μ_B per metal center and is lower than expected for a high spin d^5 system. While hyperfine splittings of ^{55}Mn ($S = 5/2$) nuclei usually dominate the EPR spectra of dimeric manganese(II) complexes and proteins, the hyperfine lines are only partially resolved in the EPR spectra of the present systems.

In methanolic solution, the EPR spectrum of $[Cu_2(ClO_4)_4(L_A)]$ consists of a broad signal without resolved hyperfine structure (Fig. 2). A weak broad half-field transition can be resolved at high microwave power. This copper complex shows $\mu_{eff} = 1.34$ μ_B per metal atom suggesting an extensive quenching of the cupric ion spin moment due to metal–metal interactions. In the EPR spectrum, linewidth broadening does not allow the resolution of hyperfine couplings. Similar EPR spectra as that of $[Cu_2(ClO_4)_4(L_A)]$ have been previously reported for other dinuclear Cu^{II} complexes [48,49].

The ligand **L_A** was subsequently reacted with (3-glycidyloxypropyl)-trimethoxysilane in dry toluene, producing a 3-propoxy-2-hydroxypropyl-silane substituent on the amide nitrogen. The new precursor was immobilized on SiO_2 by reaction at 80 °C for 24 h, leading to the **L_A·SiO$_2$** hybrid material (Scheme 1). This immobilization describes a one step procedure, instead of surface glycidylation and subsequent ligand immobilization as in previous reports [10,50]. After the silica

surface modification, Soxhlet extractions ensure that only covalently grafted ligands remain on the support corresponding to a ligand concentration of 0.5 mmol g^{-1} of silica. In the infrared spectrum of the immobilized ligand the band at 1684 cm^{-1} is attributed to the ν(C=O) (amide I) stretching vibration. Both diffuse–reflectance-FTIR and DRS data clearly indicate the preparation of the $Mn_2(L_A)\cdot SiO_2$ and $Cu_2(L_A)\cdot SiO_2$ materials.

The powder EPR spectrum of the manganese hybrid material has the same qualitative features as the corresponding non-grafted $[Mn_2(CH_3COO)_4(L_A)]$ system. Therefore, we conclude that also in the SiO_2 matrix the dinuclear manganese complexes are formed.

The immobilized $Cu_2(L_A)\cdot SiO_2$ powder has an EPR spectrum which is characteristic for magnetically coupled Cu^{2+} dimers (Fig. 2).

The well resolved $\Delta M_S = 2$ transition allows an estimation of the interspin distance to be made by using the Eqs. (2a) and (2b). By taking the integrals of the allowed and forbidden transitions for $Cu_2(L_A)\cdot SiO_2$ in Fig. 2 we obtain a ratio $[3.1 \pm 0.3] \times 10^{-3}$. The error of 10% is due to baseline uncertainty during the numerical integration of the spectra. According to the ratio-distance relationship (see Fig. 1) this ratio corresponds to a Cu···Cu distance of 4.1–4.3 Å. The EPR spectrum, due to lack of resolved hyperfine splittings, does not provide information on the coordinating atoms, however taking into account the structure of the L_A ligand, the average Cu···Cu distance of 4.2 Å fits well with coordination of two Cu atoms by the L_A ligand, if we assume that imidazole and amide nitrogens are involved with no bridging groups between the copper atoms.

Overall, the c.w. EPR data for $Cu_2(L_A).SiO_2$ show that in the immobilized complexes the Cu···Cu interactions and distances are well defined. In contrast, in solution the EPR spectrum for Cu_2L_A is less-well resolved indicating that the Cu···Cu magnetic interactions and the Cu···Cu distances are less homogeneous.

The reaction of iminodiacetic acid with 1,2-diaminobenzene results in the formation of $\mathbf{L_B}$, which bears two benzimidazole rings (Scheme 2). This ligand shows, an ESI-MS spectrum with a molecular peak $[MH]^+$ at *m/z* 278 and exhibits, in the IR-region 1645–1439 cm^{-1}, bands attributable to the benzimidazole vibrations. ^1H and ^{13}C NMR data clearly demonstrate the formation of a symmetrical ligand molecule. In the near-UV region, the electronic spectrum of $\mathbf{L_B}$ comprised absorptions at 239, 271 and 279 nm due to the $\pi \rightarrow \pi^*$ transitions in the benzimidazole rings.

The interaction of $\mathbf{L_B}$ with Mn(II) and Cu(II) ions leads to the formation of the corresponding mononuclear complexes through coordination of the central amine and the benzimidazole rings. The UV–vis spectra of the $[Mn(CH_3COO)_2(L_B)]\cdot H_2O$ and $[Cu(ClO_4)_2(L_B)]\cdot H_2O$ complexes display absorptions at 248, 276, 287 and 247, 278, 289 and 684 nm, respectively. In methanolic solution, the EPR spectrum of $[Cu(ClO_4)_2L_B]$ (see Fig. 2) is typical for mononuclear Cu^{2+} complexes with d_{x2-y2} ground state [51]. No half-field transition can be resolved in frozen solution EPR spectrum (see Fig. 2). Computer simulation of the spectrum gives the following parameters $g_{||} = 2.27$, $g_{\perp} = 2.07$, $A_{||} = 152$ G. The $g_{||}$ and $A_{||}$ values indicate that the copper atom is coordinated by at least two nitrogen atoms [52].

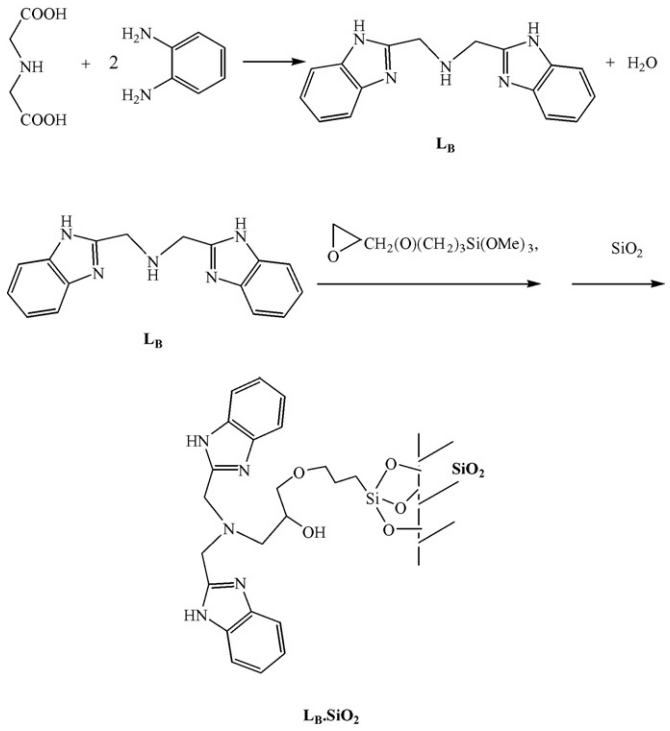

Scheme 2. Synthesis and immobilization of the ligand L_B.

Immobilization of the ligand $\mathbf{L_B}$ on SiO_2 surface occurs via its reaction with (3-glycidyloxypropyl)-trimethoxysilane in the presence of SiO_2, providing the $\mathbf{L_B}\cdot\mathbf{SiO_2}$ hybrid material (Scheme 2). This procedure is analogous to those described for immobilization of $\mathbf{L_A}$. The loading achieved is ca. 0.5 mmol g^{-1}, as determined by thermogravimetric analysis, and the diffuse reflectance UV spectrum of the material shows bands at 232, 274 and 286 nm. The observed shifts of these bands relative to those of the non-immobilized ligand are a common feature for $\pi \rightarrow \pi^*$ transitions in modified materials and they could indicate ligand-silica matrix interactions changing the donor ability of the ligand [53].

In the DRS spectra, the obtained $Mn(L_B)\cdot SiO_2$ and $Cu(L_B)\cdot SiO_2$ materials exhibit bands at 250, 278, 292 and 251, 279, 294 and 687 nm, respectively. These bands are positively shifted relative to those of the immobilized ligand due to the coordination of the metal ions.

The immobilized $Cu(L_B)\cdot SiO_2$ powder has an EPR spectrum shows resolved $\Delta M_S = 2$ transition, (see Fig. 2). By taking the integrals of the allowed and forbidden transitions for $Cu(L_B)\cdot SiO_2$ powder in Fig. 2 we obtain a ratio of $[1.1 \pm 0.3] \times 10^{-3}$. According to the ratio-distance relationship (see Fig. 1) this corresponds to a Cu···Cu distance of 4.8–5.3 Å. This Cu···Cu distance cannot be accommodated for two Cu atoms per L_B ligand. As we show in the 2D-HYSCORE spectrum of the immobilized $Cu(L_B)\cdot SiO_2$ (see Supporting information), the Cu atom is coordinated by the imidazole nitrogens from the benzimidazole. Thus we conclude that in the immobilized $Cu(L_B)\cdot SiO_2$ the Cu···Cu interaction originates from neighbouring *monomeric* CuL_B complexes which are grafted on the SiO_2 particle at average distances near 5.2 Å.

Structural information from the HYSCORE data (see Supporting information) shows that (a) in immobilized $Cu(L_B)\cdot SiO_2$ as well as in $Cu(L_B)$ in methanol, the imino nitrogen of the benzimidazole ring is coordinated to the Cu^{2+}. This is in accordance with the c.w. EPR which indicates the existence of nitrogen ligands in the coordination sphere of Cu(II). (b) In both cases, only monomeric Cu(II) complexes exist with no connecting atoms between them, such as H-bonds or bridging solvent molecules. Despite that, as we show in the following, the immobilized monomeric $Cu(L_B)\cdot SiO_2$ show catalytic activity which is considerably higher than the $Cu(L_B)$ in solution. Based in the c.w. EPR data we show that this activity can be correlated with the fixed geometrical proximity of the $Cu(L_B)$ complexes grafted onto the SiO_2 particles.

3.2. Catalytic properties of homogeneous and heterogenized Mn(II) complexes

Oxidations of several alkenes have been carried out at room temperature in a mixture of acetone: methanol (0.50:0.35, v/v) in the presence of Mn(II) complexes, in molar ratios of catalyst: H_2O_2:CH_3COONH_4: substrate equal to 1:2000:1000:1000. Ammonium acetate was added as a cocatalyst. This is absolutely required, as in previous cases [24], in order to produce an efficient catalytic system, even in the presence of our manganese-acetate catalysts.

The results of these experiments are reported in Table 1, where it can be observed that the Mn(II) complexes/CH_3COONH_4/H_2O_2 system led to the epoxidation of various alkenes with significant to very good yields (50–84%). For example, depending upon the nature of catalyst, the yields for cyclooctene, cyclohexene, hex-1-ene, styrene, *cis*-stilbene, isoprene and limonene epoxidation vary from 58.5–83.5%, 51.3–72.3%, 13.3–15.2%, 14.5–28.6%, 11.2–38.5%, 26.3–38.9% to 40.2–73.1%, respectively (Table 1). The obtained data for limonene epoxidation can be directly compared to those of the same reaction catalysed by the classical manganese–porphyrin systems [16]. In all cases, the epoxides formed are by far the favoured products. Products from possible cleavage of the double bond in styrene, or from allylic oxidation in alkenes have been not detected. Cyclohexene oxide or styrene oxide were found to be stable under the reaction conditions. In control experiments replacing our catalysts with $Mn(OAc)_3\cdot 3H_2O$, strong peroxide decomposition and no epoxide formation was found. Retention of alkene configuration is not absolute, since from *cis*-stilbene for instance, a 2:1 mixture of *cis* and *trans* epoxides are generally obtained.

Alkene reactivity depends on the electron density of the double bond, increasing for example from hex-1-ene to cyclohexene. In this context, the more electron-rich, methylated 1,2-double bond of isoprene is clearly preferred than the more exposed 3,4-double bond, while the electron-rich trisubstituted double bond of limonene in 1,2-position gives much more epoxides than the more accessible but less electron-rich double bond in 8,9-position. Such behaviour is in accordance with an electrophilic nature of the oxygen transfer from the putative oxomanganese-intermediate to the olefinic double bond. Moreover, it indicates that none of the used ligands, neither the inorganic matrix pose any steric hindrance preventing the access, for example, to the more electron-rich but also more hindered 1,2-double bond of limonene.

Comparing the present manganese systems with that previously reported by our group [24], we observe that the present systems are more active in the epoxidation of cyclooctene and limonene at room temperature with hydrogen peroxide, but less active in the epoxidation of isoprene, *cis*-stilbene and styrene. In addition, from the data in Table 1, the comparison of the dependence of epoxide yields on the nature of the used ligands L_A and L_B shows that the Mn-L_B catalysts exhibit higher reactivity. Such a behaviour is not likely to be due to the mononuclear nature of the Mn-L_B catalysts versus the binuclear Mn-L_A catalysts, since binuclear manganese systems, under similar conditions, are reported to favour epoxidation reactions [24]. Thus, the observed higher reactivity of the Mn-L_B catalysts

Table 1
Alkene epoxidations catalyzed by manganese complexes in the presence of H_2O_2[a]

Substrate	Products	Yield (%)[b]				Total Yield (%)[b] (TOF[c], h^{-1})			
		1	3	5	7	1	3	5	7
Cyclooctene	Epoxide					61.7 (*26*)	58.5 (*24*)	83.5 (*35*)	78.1 (*33*)
Cyclohexene	Epoxide					51.3 (*21*)	52.1 (*22*)	70.7 (*29*)	72.3 (*30*)
Hex-1-ene	Epoxide					14.1 (*6*)	13.3 (*6*)	15.2 (*6*)	13.6 (*6*)
Styrene	Epoxide					18.4 (*8*)	14.5 (*6*)	28.6 (*12*)	26.3 (*11*)
cis-Stilbene	*cis*-Epox.	10.1	7.2	26.6	17.8	15.4 (*6*)	11.2 (*5*)	38.5 (16)	26.4 (*11*)
	trans-Epox.	5.3	4.0	11.9	8.6				
Isoprene	1,2-Epox.	20.4	27.3	19.3	22.4	29.3 (*12*)	38.9 (*16*)	26.3 (11)	30.1 (*13*)
	3,4-Epox.	8.9	11.6	7.0	7.7				
Limonene[d]	*cis*-1,2-Epox.	19.4	22.6	28.8	36.8	40.2 (*17*)	46.6 (*19*)	58.5 (24)	73.1 (*30*)
	trans-1,2-Epox.	17.4	20.4	25.4	34.3				
	8,9-Epox.	3.4	3.4	4.3	2.0				

[a] Conditions: ratios of catalyst:H_2O_2:CH_3COONH_4:substrate = 1:2000:1000:1000; equivalent of catalyst = 1 μmol in 0.85 ml CH_3COCH_3:CH_3OH (0.55:0.3, v/v); reactions were usually complete within 24 h.
[b] Yields based on epoxides formed.
[c] TOF: turnover frequency which is calculated by the expression ([epoxide]/[catalyst]) × time (h^{-1}).
[d] Limonene 1,2-oxide was found as a mixture of cis and trans isomers and limonene 8,9-oxide as a mixture of two diastereoisomers.

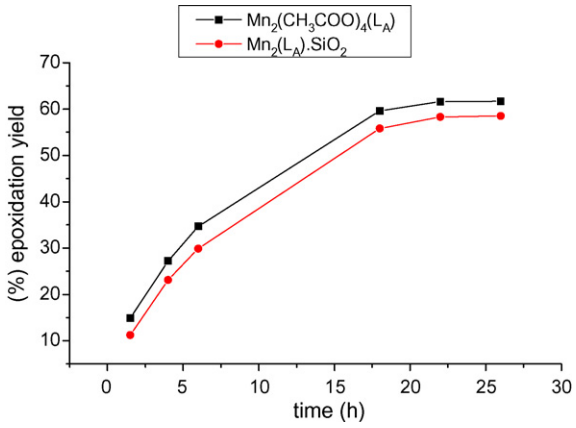

Fig. 3. Time profile of the cyclooctene epoxidation with H_2O_2 catalyzed by $[Mn_2(CH_3COO)_4(L_A)]$ and $Mn_2(L_A)\cdot SiO_2$ catalysts. Conditions: ratios of catalyst: H_2O_2:CH_3COONH_4:alkene = 1:2000:1000:1000; equivalent of catalyst = 1 μmol in 0.85 ml CH_3COCH_3:CH_3OH (0.55:0.3, v/v).

could be attributed to the generation of a more electrophilic, and thus more active, oxomanganese intermediate based on the bis-benzimidazole ligand L_B.

Evaluating the catalytic activity of the present homogeneous and heterogenized systems, we see that they very often result in similar yields; occasionally, the heterogenized catalysts exhibit slightly lower activity than the corresponding homogeneous, while in some cases, i.e. limonene epoxidation, the heterogenized systems clearly show enhanced catalytic activity than the corresponding homogeneous catalysts (Table 1). This indicates that (a) the immobilization procedure that we use does not affect the catalytic reactivity of the homogeneous catalysts and, (b) that the inorganic support does not introduce any steric hindrance preventing the substrate access to the metal sites. The latter point is further supported by the time course profiles of the Mn-L_A-catalysed epoxidations of cyclooctene and cyclohexene, which show that the amounts of both epoxides produced by the homogeneous and heterogenized catalysed reactions increase progressively with time (Figs. 3 and 4).

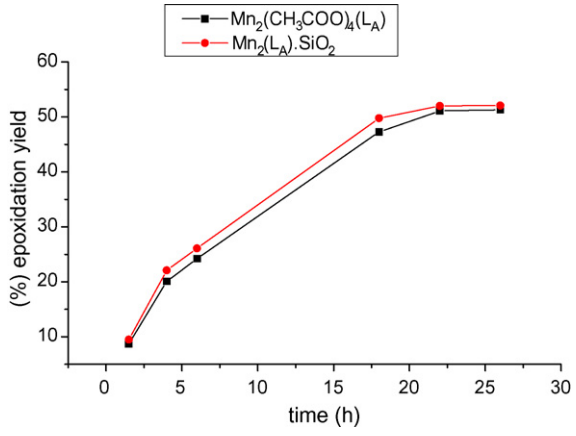

Fig. 4. Time profile of the cyclohexene epoxidation with H_2O_2 catalyzed by $[Mn_2(CH_3COO)_4(L_A)]$ and $Mn_2(L_A)\cdot SiO_2$ catalysts. Conditions:Ratios of catalyst: H_2O_2:CH_3COONH_4:alkene = 1:2000:1000:1000; equivalent of catalyst = 1 μmol in 0.85 ml CH_3COCH_3:CH_3OH (0.55:0.3, v/v).

Overall, the present supported manganese complexes are able to overcome the competitive H_2O_2 dismutation, by the use of only a double excess of H_2O_2, favouring useful alkene epoxidations to a remarkable extent.

3.3. Catalytic properties of homogeneous and heterogenized copper(II) complexes

The ability of heterogenized systems, $Cu_2(L_A)\cdot SiO_2$ and $Cu(L_B)\cdot SiO_2$, to catalyze the oxidation of 3,5-di-*tert*-butylcatechol (DTBC) was evaluated and the results were compared with those found for the catalytic reactions by the homogeneous $[Cu_2(ClO_4)_4(L_A)]$ and $[Cu(ClO_4)_2(L_B)]$ complexes. The oxidations were carried out in a methanol solution containing 100 equiv. of triethylamine, with a ratio of [catalyst]:[base]:[DTBC] equal to 0.3:30:200, always using air dioxygen as oxidant. DTBQ formation and DTBC consumption in the reactions catalysed by the present copper systems are listed in Table 2.

We observe, as in previous cases [54,55], that the catalytic reaction depends on the amount of base added. This is likely due to the fact that the added triethylamine promotes the formation of the initial dicopper–catechol complex, which is the precursor for the electron transfer process, by proton abstraction of DTBC [54] (Scheme 3).

From the data of Table 2, we note that the converted amount of DTBC does not fit in with that of the amount of formed DTBQ, showing a deviation of 1.1–10.6% that indicates that DTBQ is not the only oxidation product. Stable radical species have been detected by EPR from the catalytic mixture attributable to *o*-semiquinone radicals [55]. However, the main catalytic product of DTBC oxidation is by far the corresponding quinone DTBQ (Table 2).

Moreover, the catalytic activity of the heterogenized system $Cu_2(L_A)\cdot SiO_2$, when compared with that of the homogeneous catalyst, $[Cu_2(ClO_4)_4(L_A)]$, is further improved. Namely, $Cu_2(L_A)\cdot SiO_2$ converts 96% of DTBC while the homoge-

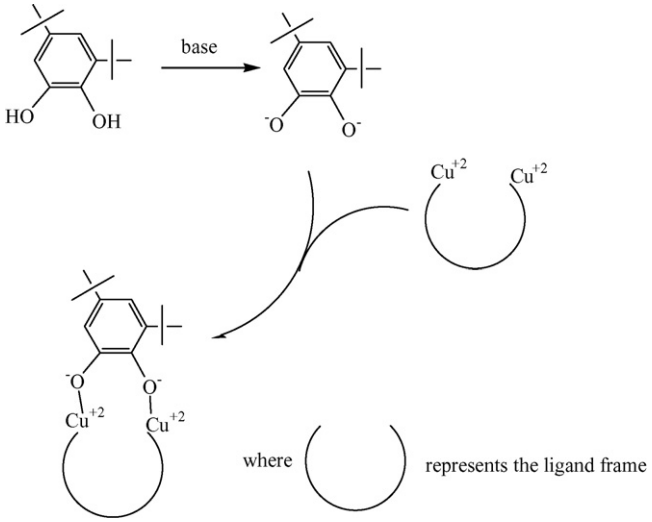

Scheme 3. The intermediate dicopper–catechol complex.

Table 2
Catalytic oxidation of 3,5-di-*t*-butylcatechol by dioxygen (catalyst:base:DTBC equal to 0.3:30:200)

Catalyst	DTBQ formation (%) (TON)[a]		DTBC conversion (%) (TON)[b]	
	24 h	48 h	24 h	48 h
$Cu_2(L_A)$	60.0 (*400*)	70.6 (*471*)	68.6 (*457*)	79.0 (*527*)
$Cu_2(L_A)\cdot SiO_2$	69.0 (*460*)	92.6 (*617*)	90.0 (*600*)	96.0 (*640*)
$Cu(L_B)$	23.0 (*153*)	37.1 (*247*)	24.5 (*163*)	38.2 (*255*)
$Cu(L_B)\cdot SiO_2$	49.7 (*331*)	78.1 (*521*)	61.4 (*409*)	88.7 (*591*)

[a] TON: moles of DTBQ formed per mole of catalyst.
[b] TON: moles of DTBC converted per mole of catalyst.

neous catalyst converts 79% in the same conditions. As for DTBQ formation, we observe that while 92.6% of DTBQ is produced by $Cu_2(L_A)\cdot SiO_2$, 70.6% of DTBQ is produced by $[Cu_2(ClO_4)_4(L_A)]$ (Table 2 and Fig. 5).

The activity of the homogeneous and heterogenized dicopper systems $[Cu_2(ClO_4)_4(L_A)]$ and $Cu_2(L_A)\cdot SiO_2$ in the DTBC catalytic oxidation by atmospheric dioxygen is noteworthy, while the mononuclear $[Cu(ClO_4)_2(L_B)]$ complex shows low catalytic activity. However, the supported mononuclear $Cu(L_B)\cdot SiO_2$ catalyst is also highly efficient.

The present catalytic data are associated with two distinct features. First, for the CuL_A system, the EPR data show that the Cu atoms are in dimeric arrangement both in solution and in the immobilized material. In the latter case, the EPR spectrum shows a well fixed geometrical arrangement with an average Cu···Cu distance of 4.2 Å. Taking into account the ionic radius of the copper atom, this Cu···Cu distance can accommodate the OC–CO distance in the DTBC molecule and this is expected to facilitate the bidentate approach and coordination of DTBC on the two, well-fixed, Cu atoms. As a result, the dimeric Cu_2L_A species shows good catalytic conversion of DTBC in solution and even better by the $Cu_2L_A\cdot SiO_2$ solid material (Table 2 and Fig. 5). Second, in the case of the homogeneous CuL_B complex, the monomeric nature of the catalyst hinders the coordination of a single substrate molecule by two different Cu centres, as the two-step mechanism of DTBC oxidation requires its sequential approach to two CuL_B complexes. This geometry-based reasoning seems to concur with the observed lower catalytic efficiency of DTBC oxidation by CuL_B than Cu_2L_A and $Cu_2(L_A)\cdot SiO_2$ (Table 2 and Fig. 5). Such correlation between catalytic activity and proper geometrical arrangement of monomeric and dimeric copper complexes is consistent with other pertinent recently published data [56].

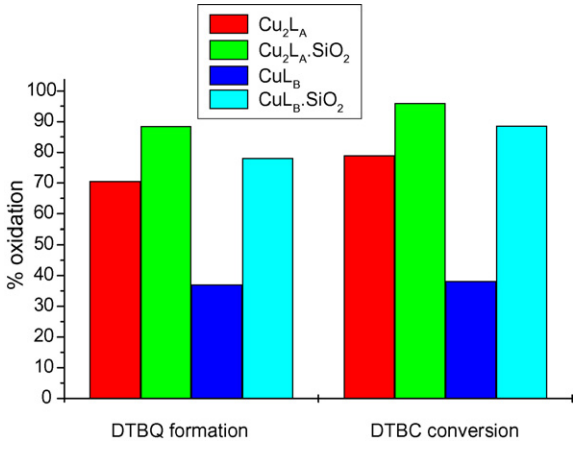

Fig. 5. Screen for DTBQ formation and DTBC conversion catalyzed by Cu(II) complexes. Condition: ratios of catalyst:base:DTBC equal to 0.3:30:200.

The immobilization of the monomeric CuL_B complex on the silica support imposes a close proximity of neighbour copper centres. Thus, the immobilized $CuL_B\cdot SiO_2$ catalyst has an average CuL_B–CuL_B distance of 5.2 Å. In this system, the adjacent CuL_B centres are in fixed positions and their separation is larger than the corresponding distance of 4.2 Å in the $Cu_2(L_A)\cdot SiO_2$. However, this Cu···Cu proximity seems to be crucial in offering a marked enhancement of catalytic activity towards DTBC oxidation (Table 2 and Fig. 5).

Overall, among the factors that play a role in the DTBC catalytic oxidation, we point out the dependence on basic conditions and the relative disposition of the active copper pairs. The silica support appears to promote the proximity between metal centres, probably due to space restriction, resulting in the observed higher reactivity of the heterogenized systems. In this context, the loading of the SiO_2 particles is expected to play a primary role, since it will determine the density and the geometrical proximity of the immobilized complexes. Experiments are in progress in our lab to investigate this effect.

4. Conclusions

We have synthesized two new ligands and subsequently they were grafted on a silica surface via covalent bonds. The corresponding manganese(II) and copper(II) complexes with the organic ligands as well as with the heterogenized ligands have been also prepared.

The manganese complexes were evaluated as oxidation catalysts for the epoxidation of simple olefins with hydrogen peroxide. The results obtained here demonstrate that homogeneous and supported manganese complexes are able to overcome the competitive H_2O_2 dismutation, by the use of only a double excess of H_2O_2, favouring useful alkene epoxidations to a remarkable extent. This indicates that the active catalytic features of the homogeneous systems were successfully diffused onto the silica surface providing efficient heterogenized systems. However, the presence of ammonium acetate, as cocatalyst, is absolutely required to incorporate hydrogen peroxide, even here by using manganese-acetate-based catalysts.

The ability of copper(II) complexes to promote the catalytic oxidation of DTBC by dioxygen was tested. Based on catalytic data in conjunction with EPR information, we suggest that a determining factor for efficient DTBC conversion is the Cu···Cu distance. In cases where the Cu···Cu distance from the same or neighbouring complexes can accommodate the OC···CO byte in catechol (2.7 Å between the two O atoms' geometrical centers) this facilitates a bidentate coordination of DTBC on two, well-fixed, Cu atoms. In this context, immobilization of the copper catalysts enhances catalytic conversion of DTBC even in cases where monomeric copper complexes are grafted at distances approaching the critical OC···CO distance of 2.7 Å. Work is in progress to further clarify this critical factor, so that efficient DTBC oxidation can be predicted by examining the metal sites involved in the catalytic sites.

Acknowledgement

D. Zois gratefully acknowledges the Marie Curie Training Site "MEBIOS" for a fellowship. The authors thank financial support from the University of Pavia (through FAR) and the program "Heraklitos" in the framework of the "Operational Program for Education and Initial Vocational Training" of the 3rd Community Support Framework of the Hellenic Ministry of Education, funded by 25% from national sources and by 75% from the European Social Fund (ESF).

Appendix A. Supplementary data

Supplementary data associated with this article can be found, in the online version, at doi:10.1016/j.molcata.2006.11.023.

References

[1] J.H. Clark, Green Chem. 1 (1999) 1–8.
[2] A.P. Wight, M.E. Davis, Chem. Rev. 102 (2002) 3589–3613.
[3] C.E. Song, S-g. Lee, Chem. Rev. 102 (2002) 3495–3524.
[4] J.H. Clark, D.J. Macquarrie, Chem. Commun. (1998) 853–854.
[5] H.H. Weetall, in: K. Mosbach (Ed.), Methods in Enzymology, vol. 44, Academic Press, New York, 1976, pp. 134–148.
[6] S.K. Bhatia, L.C. Shriver-Lake, J.H. Georger, J.M. Calvert, R. Bredehorst, F.S. Ligler, Anal. Biochem. 178 (1989) 408–413.
[7] C. Brüning, J. Grobe, Chem. Comm. (1995) 2323–2324.
[8] A.J. Butterworth, J.H. Clark, P.H. Walton, S.J. Barlow, Chem. Comm. (1996) 1859–1860.
[9] G.M. Kloster, C.M. Taylor, S.P. Watton, Inorg. Chem. 38 (1999) 3954–3955.
[10] Y.V.S. Rao, D.E. De Vos, T. Bein, P.A. Jacobs, Chem. Comm. (1997) 355–356.
[11] R.J. Clarke, I.J. Shannon, Chem. Comm. (2001) 1936–1937.
[12] D. Brunel, A. Cauvel, F. Di Renzo, F. Fajula, B. Fubini, B. Onida, E. Garrone, New J. Chem. 24 (2000) 807–813.
[13] F. Fache, E. Schulz, M.L. Tommasino, M. Lemaire, Chem. Rev. 100 (2000) 2159–2231.
[14] F. Adrian, M.I. Burguete, J.M. Fraile, J.I. Garcia, J. Garcia, E. Garcia-Espana, S.V. Luis, J.A. Mayoral, A.J. Royo, M.C. Sanchez, Eur. J. Inorg. Chem. (1999) 2347–2354.
[15] B. Meunier, Biomimetic Oxidations Catalyzed by Transition Metal Complexes, Imperial College Press, London, 2000.
[16] P. Battioni, J.P. Renaud, J.F. Bartoli, M. Reina-Artiles, M. Fort, D. Mansuy, J. Am. Chem. Soc. 110 (1988) 8462–8470.
[17] E.N. Jacobsen, in: I. Ojima (Ed.), Catalytic Asymmetric Synthesis, VCH, New York, 1993.
[18] E.N. Jacobsen, W. Zhang, A.R. Muci, J.R. Ecker, L. Deng, J. Am. Chem. Soc. 113 (1991) 7063–7064.
[19] K. Bernardo, S. Leppard, A. Robert, G. Commenges, F. Dahan, B. Meunier, Inorg. Chem. 35 (1996) 387–396.
[20] P.-P. Knops-Gerrits, D. De Vos, F. Thibault-Starzyk, P.A. Jacobs, Nature 369 (1994) 543–546.
[21] R. Hage, J.E. Iburg, J. Kerschner, J.H. Keek, E.L.M. Lempers, R.J. Martens, U.S. Racherla, S.W. Russel, T. Swarthoff, M.R.P. van Vliet, J.B. Warnaar, L. van der Wolf, B. Krijnen, Nature 369 (1994) 637–639.
[22] D. De Vos, T. Bein, Chem. Commun. (1996) 917–918.
[23] J. Brinksma, R. Hage, J. Kerschner, B.L. Feringa, Chem. Commun. (2000) 537–538.
[24] Ch. Kolokytha, M. Louloudi, N. Hadjiliadis, J. Mol. Catal. A 180 (2002) 19–24.
[25] M.A. Martinez-Lorente, P. Battioni, W. Kleemiss, J.F. Bartoli, D. Mansuy, J. Mol. Catal. A 113 (1996) 343–353.
[26] M.R. Malachowski, H.B. Huynh, L.J. Tomlinson, R.S. Kelly, J.W. Furbee Jr., J. Chem. Soc. Dalton Trans. (1995) 31–36.
[27] M. Louloudi, Y. Deligiannakis, N. Hadjiliadis, Inorg. Chem. 37 (1998) 6847–6851.
[28] T.N. Sorrell, V.A. Vankai, M.L. Garity, Inorg. Chem. 30 (1991) 210–215.
[29] T.N. Sorrell, W.E. Allen, P.S. White, Inorg. Chem. 34 (1995) 952–960.
[30] F. Zippel, F. Ahlers, R. Werner, W. Haase, H.-F. Nolting, B. Krebs, Inorg. Chem. 5 (3) (1996) 3409–3419.
[31] J. Reim, B. Krebs, J. Chem. Soc. Dalton Trans. (1997) 3793–3804.
[32] E. Monzani, L. Quinti, A. Perotti, L. Casella, M. Gullotti, L. Randaccio, S. Geremia, G. Nardin, P. Faleschini, G. Tabbi, Inorg. Chem. 37 (1998) 553–562.
[33] E. Monzani, G. Battaini, A. Perotti, L. Casella, M. Gullotti, L. Santagostini, G. Nardin, L. Randaccio, S. Geremia, P. Zanello, G. Opromolla, Inorg. Chem. 38 (1999) 5359–5369.
[34] S. Torelli, C. Belle, S. Hammam, J.-L. Pierre, Inorg. Chem. 41 (2002) 3983–3989.
[35] S.A. Dikanov, Y.D. Tsvetkov, ESEEM Spectroscopy, CRC Press, Boca Raton, 1992.
[36] G. Malandrinos, M. Louloudi, Y. Deligiannakis, N. Hadjiliadis, J. Phys. Chem. B 105 (2001) 7323–7333.
[37] P. Höfer, A. Grupp, H. Nebenführ, M. Mehring, Chem. Phys. Lett. 132 (1986) 279–282.
[38] Y. Deligiannakis, M. Louloudi, N. Hadjiliadis, Coord. Chem. Rev. 204 (2000) 1–112.
[39] A. Pöppl, L. Kevan, J. Phys. Chem. 100 (1996) 3387–3394.
[40] A. Bencini, D. Gatteschi, EPR of Exchange Coupled Systems, Springer-Verlag, Berlin, 1990.
[41] P.J. Hay, J.C. Thibeault, R. Hoffmann, J. Am. Chem. Soc. 97 (1975) 4884–4899.
[42] D.N. Hendrickson, in: R.D. Willet, D. Gatteschi, O. Kahn (Eds.), Magneto-Structural Correlations in Exchange Coupled Systems, NATO ASI Series, Reidel Publishing Company, Dordrecht, 1983, pp. 497–555.
[43] S. Eaton, K.M. More, B.M. Sawant, G.R. Eaton, J. Am. Chem. Soc. 105 (1983) 6560–6567.
[44] R.E. Coffman, A. Pezeshk, J. Magn. Res. 70 (1986) 21–33.
[45] S. Eaton, G.R. Eaton, C.K. Chang, J. Am. Chem. Soc. 107 (1985) 3177–3184.
[46] M.H. Valkenberg, W.F. Hölderich, Catal. Rev. 44 (2002) 321–374.
[47] A. Gelasco, M.L. Kirk, J.W. Kampf, V.L. Pecoraro, Inorg. Chem. 36 (1997) 1829–1837.
[48] C.F. Martens, A.P.H.J. Schenning, M.C. Feiters, J. Heck, P.T. Beurskens, E. Steinwender, R.J.M. Nolte, Inorg. Chem. 32 (1993) 3029–3033.
[49] M. Klein, R.J.M. Gebbink, C.F. Martens, P.J.A. Kenis, R.J. Jansen, H.-F. Nolting, V.A. Sole, M.C. Feiters, K.D. Karlin, R.J.M. Nolte, Inorg. Chem. 38 (1999) 5755–5768.
[50] P.M. van Berkel, W.L. Driessen, G.J.A.A. Kodhaas, J. Reedijk, D.C. Sherrington, J. Chem. Soc., Chem. Commun. (1995) 147–148.
[51] J.R. Pilbrow, Transition Ion Electron Paramagnetic Resonance, Clarendon Press, Oxford, 1990.

[52] J. Peisach, W.E. Blumberg, Arch. Biochem. Biophys. 165 (1974) 691–708.
[53] R. Ferreira, M. Silva, C. Freire, B. de Castro, J.L. Figueiredo, Microp. Mesop. Mater. 38 (2000) 391–401.
[54] M. Louloudi, K. Mitopoulou, E. Evaggelou, Y. Deligiannakis, N. Hadjiliadis, J. Mol. Catal. A 198 (2003) 231–240.
[55] C.H. Lee, S.T. Wong, T.S. Lin, C.Y. Mou, J. Phys. Chem. B 109 (2005) 775–784.
[56] M. Gullotti, L. Santagostini, R. Pagliarin, A. Granata, L. Casella, J. Mol. Catal.: A Chem. 235 (2005) 271–284.